JGR Space Physics

METHOD

10.1029/2025JA034868

Daily Predictions of F10.7 and F30 Solar Indices With Deep Learning

Zhenduo Wang[1,2], Yasser Abduallah[1,2], Jason T. L. Wang[1,2], Haimin Wang[1,3,4], Yan Xu[1,3,4], Vasyl Yurchyshyn[4], Vincent Oria[1,2], Khalid A. Alobaid[5], and Xiaoli Bai[6]

[1]Institute for Space Weather Sciences, New Jersey Institute of Technology, Newark, NJ, USA, [2]Department of Computer Science, New Jersey Institute of Technology, Newark, NJ, USA, [3]Center for Solar-Terrestrial Research, New Jersey Institute of Technology, Newark, NJ, USA, [4]Big Bear Solar Observatory, New Jersey Institute of Technology, Big Bear City, CA, USA, [5]College of Applied Computer Sciences, King Saud University, Riyadh, Saudi Arabia, [6]Department of Mechanical and Aerospace Engineering, Rutgers University, Piscataway, NJ, USA

Key Points:

- We present a deep learning model, named SINet, for making daily predictions of F10.7 and F30 solar indices (1–60 days in advance)
- SINet outperforms five closely related statistical and deep learning methods for F10.7 prediction
- SINet is the first deep learning method for F30 prediction

Correspondence to:

J. T. L. Wang and H. Wang,
wangj@njit.edu;
haimin.wang@njit.edu

Citation:

Wang, Z., Abduallah, Y., Wang, J. T. L., Wang, H., Xu, Y., Yurchyshyn, V., et al. (2026). Daily predictions of F10.7 and F30 Solar indices with deep learning. *Journal of Geophysical Research: Space Physics*, *131*, e2025JA034868. https://doi.org/10.1029/2025JA034868

Received 10 NOV 2025
Accepted 26 JAN 2026

Author Contributions:

Conceptualization: Jason T. L. Wang, Haimin Wang, Yan Xu, Vasyl Yurchyshyn, Xiaoli Bai
Data curation: Zhenduo Wang, Yan Xu, Vasyl Yurchyshyn, Khalid A. Alobaid
Formal analysis: Zhenduo Wang, Jason T. L. Wang
Funding acquisition: Jason T. L. Wang, Haimin Wang, Xiaoli Bai
Investigation: Zhenduo Wang, Jason T. L. Wang, Haimin Wang
Methodology: Zhenduo Wang, Yasser Abduallah, Jason T. L. Wang
Project administration: Yasser Abduallah, Jason T. L. Wang, Haimin Wang, Vincent Oria, Xiaoli Bai
Resources: Yasser Abduallah, Jason T. L. Wang, Haimin Wang, Yan Xu, Vasyl Yurchyshyn, Vincent Oria, Khalid A. Alobaid, Xiaoli Bai
Software: Zhenduo Wang, Yasser Abduallah
Supervision: Jason T. L. Wang, Haimin Wang, Xiaoli Bai
Validation: Zhenduo Wang, Yasser Abduallah, Jason T. L. Wang, Haimin Wang, Yan Xu, Vasyl Yurchyshyn
Visualization: Zhenduo Wang, Vasyl Yurchyshyn, Vincent Oria

Abstract The F10.7 and F30 solar indices are the solar radio fluxes measured at wavelengths of 10.7 and 30 cm, respectively, which are key indicators of solar activity. F10.7 is valuable for explaining the impact of solar ultraviolet (UV) radiation on the upper atmosphere of Earth, while F30 is more sensitive and could improve the reaction of thermospheric density to solar stimulation. In this study, we present a new deep learning model, named the Solar Index Network, or SINet for short, to predict daily values of the F10.7 and F30 solar indices. The SINet model is designed to make medium-term predictions of the index values (1–60 days in advance). The observed data used for SINet training were taken from the National Oceanic and Atmospheric Administration as well as Toyokawa and Nobeyama facilities. Our experimental results show that SINet performs better than five closely related statistical and deep learning methods for the prediction of F10.7. Furthermore, to our knowledge, this is the first time deep learning has been used to predict the F30 solar index.

Plain Language Summary F10.7 and F30 are key indices that reflect the level of solar activity. F10.7 is valuable for explaining the impact of solar ultraviolet (UV) radiation on the upper atmosphere of Earth, while F30 is more sensitive and could improve the reaction of thermospheric density to solar stimulation. We introduce a new forecasting model, named SINet, to make medium-term daily predictions of the F10.7 and F30 solar indices. The forecast horizons range from 1 to 60 days. Our experimental results show that SINet achieves an average mean absolute percentage error (MAPE) of 10.1% for F10.7% and 9.5% for F30 at the 60th day of forecast, better than the average MAPE of 10.4% for F10.7% and 9.6% for F30 obtained by the best one (temporal convolutional network) of five closely related methods.

1. Introduction

The F10.7 and F30 solar indices refer to the solar radio fluxes measured at wavelengths of 10.7 and 30 cm, respectively. They are critical gauges of solar activity, reflecting the intensity of radio emissions from the Sun's corona (Girazian & Withers, 2015; Petrova et al., 2021; K. Zhang et al., 2024). These indices are measured in solar flux units (sfu), where 1 sfu is equal to 10^{-22}Wm^{-2}Hz^{-1}. They range from less than 50 sfu to more than 300 sfu. F10.7 is valuable for explaining the impact of solar ultraviolet (UV) radiation on the upper atmosphere of Earth, while F30 is more sensitive and could improve the reaction of thermospheric density to solar stimulation (Dudok de Wit & Bruinsma, 2017). Although F10.7 is commonly used in space weather forecasting (Tapping, 2013), some researchers recommend using F30 as the optimal proxy for solar activity (Laštovička & Burešová, 2023).

Many techniques have been developed to forecast the F10.7 and F30 solar indices. For example, Warren et al. (2017) developed a linear forecasting model to predict F10.7. Lei et al. (2019) constructed an empirical model to predict F10.7 using extreme ultraviolet images. Petrova et al. (2021) utilized the adaptive Kalman filter to improve the McNish-Lincoln method to predict F10.7 and F30. These traditional methods could be used to capture some features of the F10.7 and F30 indices but often rely on assumptions that limit their ability to capture complex, non-linear dynamics inherent in solar activity.

With the advent of deep learning, predictive models have advanced in forecast accuracy and model performance (Abduallah et al., 2023; Alobaid et al., 2024; Bernoux et al., 2022; Tasistro-Hart et al., 2021). For example, Zhu

Writing – original draft: Zhenduo Wang
Writing – review & editing: Jason T. L. Wang, Haimin Wang, Khalid A. Alobaid, Xiaoli Bai

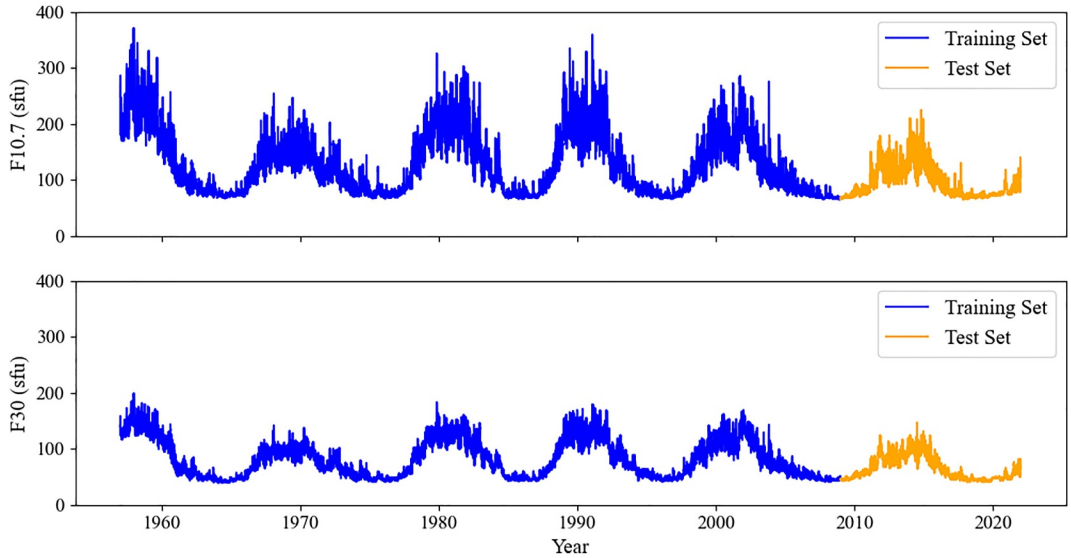

Figure 1. Illustration of the time series data sets for F10.7 (top) and F30 (bottom) used in our study.

et al. (2022) developed a long short-term memory (LSTM) network to predict F10.7 with good results. Jerse and Marcucci (2024) later designed an LSTM network with multihead attention mechanisms to predict F10.7. Daniell and Mehta (2023) used neural network ensembles to predict F10.7. Hao et al. (2024) combined an LSTM network with variational mode decomposition to make predictions of F10.7 (1 day in advance). K. Zhang et al. (2024) adopted the informer model to forecast F10.7 for up to 27 days. More recently, Wang et al. (2024) employed a deep temporal convolutional network (TCN) to make predictions of the F10.7 index. TCN has also been used to predict other solar events (see, e.g., Xu et al., 2025).

In this study, we propose a new deep learning model, named the Solar Index Network, or SINet for short, to make medium-term daily predictions of the F10.7 and F30 solar indices (1–60 days in advance). In general, short-term prediction has a forecast horizon of several days (up to one solar rotation, that is, up to 30 days). Medium-term prediction refers to predictions made one to several months in advance. Long-term prediction is made over a decade or more. Petrova et al. (2021) was able to use a traditional method, namely the adaptive Kalman filter, to predict the F10.7 and F30 solar indices 24 months in advance. However, the data they used for the predictions are monthly mean data for the F10.7 and F30 indices. The ratio between the largest forecast horizon and the cadence of the data is 24:1. K. Zhang et al. (2024) used a deep learning method to make daily predictions of F10.7 (1–27 days in advance). The ratio between their largest forecast horizon and the cadence of the data is 27:1. In contrast, our SINet model can make medium-term daily predictions of F10.7 and F30 (1–60 days in advance). The ratio between the largest forecast horizon and the cadence of the data is 60:1, far exceeding the ratios of the existing methods. We attribute the ability to handle this large ratio to the deep architecture employed by SINet.

The remainder of this paper is organized as follows. Section 2 describes the data collection and pre-processing for our work. Section 3 presents the architecture and configuration details of the SINet model. Section 4 reports the experimental results. Section 5 presents a discussion of the results. Section 6 concludes the article.

2. Data

The daily values of the F10.7 solar index are obtained from the National Oceanic and Atmospheric Administration (NOAA) as in Hao et al. (2024). The daily values of the F30 solar index are collected from the Toyokawa and Nobeyama facilities as in Petrova et al. (2021). These daily values form a one-dimensional (1D) time series that spans 1957 to 2021. The time series data are divided into training data from 1957 to 2008, 10% of which are used for validation, and test data from 2009 to 2021. Figure 1 illustrates the time series data sets for F10.7 (top) and F30 (bottom), respectively. The training set and the test set for F10.7 (F30, respectively) are disjoint. Thus, our SINet model is trained with data different from the test data and makes predictions on the test data that it has never seen during training.

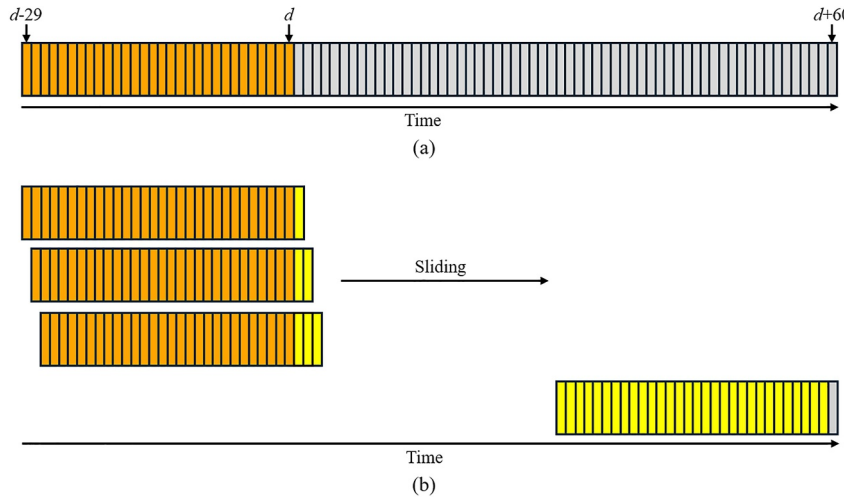

Figure 2. Illustration of the two prediction approaches employed by SINet. (a) The fixed prediction approach uses the historical F10.7 values of the previous 30 days, $d-30+1, d-30+2, \ldots, d-1, d$ Represented by orange rectangles, to predict the F10.7 values on days $d+1, d+2, \ldots, d+59, d+60$, represented by gray rectangles. (b) The rolling prediction approach uses a sliding window method, where each predicted value is appended iteratively to generate new predictions one day at a time, ultimately achieving a 60-day ahead forecast. Orange rectangles represent true historical F10.7 values, while yellow rectangles represent predicted synthetic F10.7 values that are used subsequently to make new predictions. See text for detailed descriptions of the rolling prediction approach.

Since the F10.7 data have different scales, we normalize the F10.7 data using the min-max method, which is defined as follows:

$$X_{\text{norm}} = \frac{X - X_{\text{min}}}{X_{\text{max}} - X_{\text{min}}}. \tag{1}$$

Here, X represents a daily value of F10.7, X_{norm} represents the normalized value of X, X_{min} is the minimum value of F10.7, and X_{max} is the maximum value of F10.7. The min-max normalization method produces daily F10.7 values in the range between 0 and 1. The F30 data are normalized similarly.

Data labeling is crucial for machine learning. In the following, we describe how to label the F10.7 data. The F30 data are labeled similarly, and its description is omitted. We present two different approaches: fixed prediction and rolling prediction. Consider each time point/day d in the training set. We create a training sample at the time point d that contains the historical F10.7 values for the previous 30 days. That is, the training sample contains the true F10.7 values on days $d-30+1, d-30+2, \ldots, d-1, d$. For fixed prediction, the labels of the training sample contain the true F10.7 values on days $d+1, d+2, \ldots, d+59, d+60$ (1–60 days in advance). For rolling prediction, the label of the training sample is the true F10.7 value on day $d+1$ (1 day in advance).

Next, look at each time point/day d in the test set. We create a test sample at the time point d that contains the historical F10.7 values for the previous 30 days. The labels of the test sample are absent and will be predicted by SINet. Specifically, we use the historical F10.7 values for the previous 30 days to predict the F10.7 values (1–60 days in advance). Figure 2a illustrates the fixed prediction approach. The 30 orange rectangles represent the historical F10.7 values of the previous 30 days: $d-30+1, d-30+2, \ldots, d-1, d$. The 60 Gy rectangles represent the predicted values of F10.7 on days $d+1, d+2, \ldots, d+59, d+60$.

Figure 2b illustrates the rolling prediction approach, where a sliding window method is used. We move to the right one position/day at a time, and in each step we use the historical F10.7 values of the previous 30 days to predict the next F10.7 value (1 day in advance). Initially, in step 1, we use the historical F10.7 values of the previous 30 days, represented by orange rectangles, to predict the F10.7 value (1 day in advance) on day $d+1$, represented by a yellow rectangle. Then, in step i, $2 \le i \le 30$, we use the historical F10.7 values of the previous $(30-i+1)$ days, represented by orange rectangles, combined with the $(i-1)$ predicted synthetic values obtained in the previous $(i-1)$ steps, represented by yellow rectangles, to predict the F10.7 value (1 day in advance) on day $d+i$,

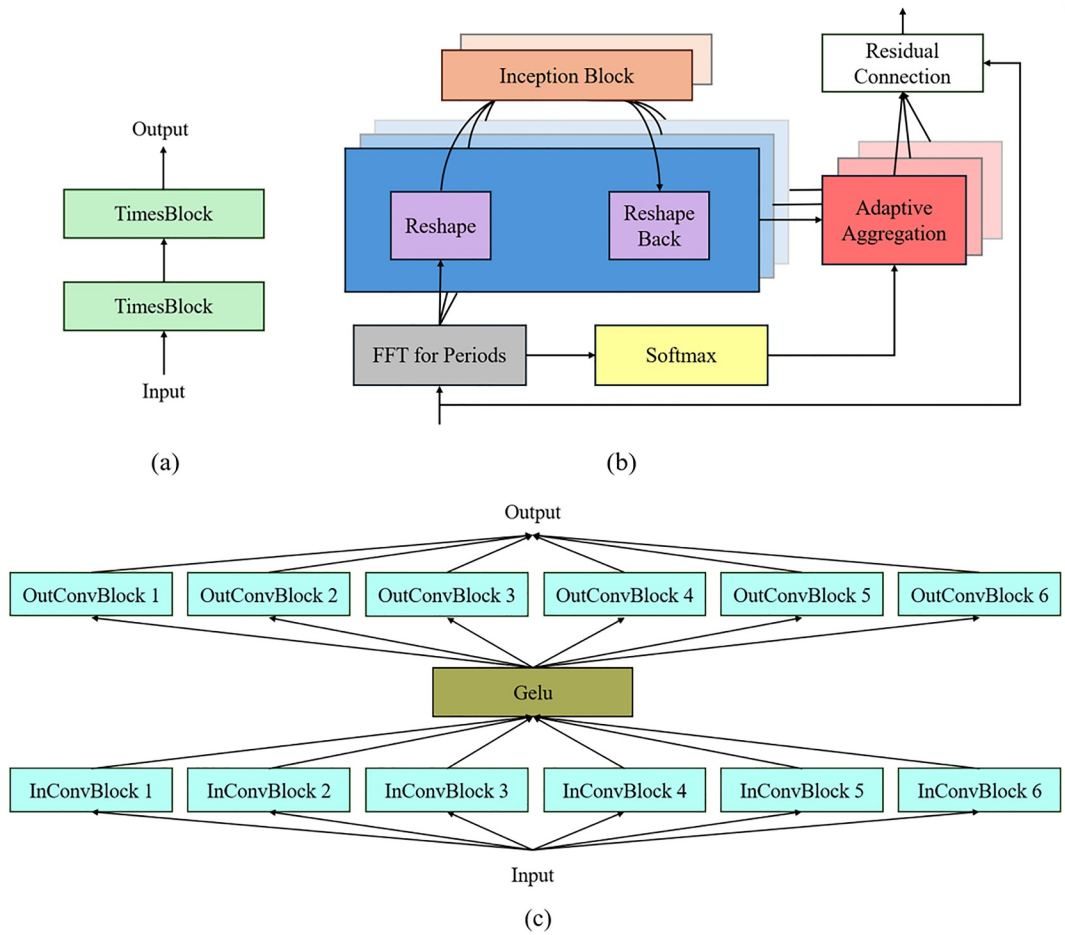

Figure 3. Illustration of the SINet model architecture. (a) Overall architecture of SINet, which contains two TimesBlocks. (b) Architecture of a TimesBlock, which contains a dual-inception model structure with two inception blocks. (c) Architecture of the dual-inception model structure, in which the two inception blocks are connected by a Gelu layer. See text for detailed descriptions of the components of SINet.

represented by a yellow rectangle. In step j, $31 \le j \le 59$, we use the synthetic F10.7 values obtained in step $(j - 30)$ to step $(j - 1)$ to predict the F10.7 value (1 day in advance) on day $d + j$. In step 60, we use the synthetic F10.7 values of the previous 30 days, represented by yellow rectangles, obtained in step 30 to step 59, to predict the F10.7 value (1 day in advance) on day $d + 60$, represented by a gray rectangle.

3. Methodology

Figure 3a shows the architecture of SINet, which is an enhancement of TimesNet (Wu et al., 2023), adapted for the prediction of solar indices. SINet employs two TimesBlocks. Each TimesBlock is designed to process 1D time series and enhance feature representation. During prediction/testing, the SINet input is a test sample with historical values of F10.7 or F30 on the previous 30 days: $d - 30 + 1, d - 30 + 2, \ldots, d - 1, d$. For the fixed prediction approach, the SINet output consists of the predicted values of F10.7 or F30 for the next 60 days: $d + 1$, $d + 2, \ldots, d + 59, d + 60$. For the rolling prediction approach, the SINet output is the predicted value of F10.7 or F30 on day $d + 1$ (1 day in advance). We then use the sliding window method described in Section 2 to iteratively predict the values of F10.7 or F30 on day $d + 2$ to day $d + 60$.

Figure 3b presents the details of a TimesBlock. The input 1D time series data are first processed by a fast Fourier transform (FFT) algorithm that converts the time domain to the frequency domain. The main purpose of the FFT algorithm is to identify and analyze periodic components within the data, specifically isolating the k most significant periodic components, where k is a user-determined parameter (In the study presented here, k is set to 3). In

Table 1
Configuration Details of the Dual-Inception Model Structure in SINet

Layer	Input dimension	Kernel size	Output dimension
InConvBlock 1	30 × 32	1 × 1	30 × 64
InConvBlock 2	30 × 32	3 × 3	30 × 64
InConvBlock 3	30 × 32	5 × 5	30 × 64
InConvBlock 4	30 × 32	7 × 7	30 × 64
InConvBlock 5	30 × 32	9 × 9	30 × 64
InConvBlock 6	30 × 32	11 × 11	30 × 64
Activation (Gelu)	30 × 64	—	30 × 64
OutConvBlock 1	30 × 64	1 × 1	30 × 32
OutConvBlock 2	30 × 64	3 × 3	30 × 32
OutConvBlock 3	30 × 64	5 × 5	30 × 32
OutConvBlock 4	30 × 64	7 × 7	30 × 32
OutConvBlock 5	30 × 64	9 × 9	30 × 32
OutConvBlock 6	30 × 64	11 × 11	30 × 32

this way, the model can focus on the important features to enhance learning effectiveness. After FFT, the k most significant periods are reshaped into k 2-dimensional (2D) tensors simultaneously, which are then sent to a dual-inception model structure containing two inception blocks. The first inception block processes the reshaped data to extract hierarchical temporal features using multiscale 2D convolutional kernels. These features are then refined by the second inception block, which further processes the data, reduces the dimensionality of the data, and prepares the data for reconstruction. After feature extraction by the inception blocks, the data are reshaped back into 1D time series, prepared for adaptive aggregation. This dual-inception model structure enables TimesBlock to effectively capture both short- and long-term dependencies in the 1D time series data.

Separately, the output of the FFT algorithm is processed by a softmax function to calculate the softmax weights, which indicate the significance of each periodic component. The k adaptive aggregation modules for the k periodic components take as input the reshaped 1D time series data together with the softmax weights, and produce as output aggregated 1D time series data. Finally, the aggregated 1D time series data is combined with the original input of the TimesBlock through a residual connection. The residual connection prevents overfitting and improves generalization.

Figure 3c presents the details of the dual-inception model structure, which is composed of two inception blocks. The first inception block consists of six in-convolution blocks (InConvBlock 1, InConvBlock 2, InConvBlock 3, InConvBlock 4, InConvBlock 5, InConvBlock 6). Each in-convolution block increases the dimension (i.e., the number of channels) in the block. The second inception block consists of six out-convolution blocks (OutConvBlock 1, OutConvBlock 2, OutConvBlock 3, OutConvBlock 4, OutConvBlock 5, OutConvBlock 6). Each out-convolution block decreases the dimension in the block. The two inception blocks are connected by a Gaussian error linear unit (Gelu) layer. Table 1 presents the configuration details of the dual-inception model structure for the medium-term daily prediction of the F10.7 and F30 solar indices (1–60 days in advance). Using validation data for performance assessment, the best forecast result is achieved using historical values of the previous 30 days to predict the future values of F10.7 and F30 (1–60 days in advance). Thus, the input (output, respectively) dimension of each in-convolution block is represented by $30 \times C$ where $C = 32$ is the number of input channels ($C = 64$ is the number of output channels, respectively) in the in-convolution block. The input (output, respectively) dimension of each out-convolution block is represented by $30 \times C$ where $C = 64$ is the number of input channels ($C = 32$ is the number of output channels, respectively) in the out-convolution block.

SINet is trained for 10 epochs, with a batch size of 32. We use the adaptive moment estimation (Adam) optimizer (Kingma & Ba, 2015) with a learning rate of 0.001, the mean square error (MSE) as the loss function, and a dropout rate of 0.3 to prevent overfitting. Table 2 summarizes the model training conditions of SINet. The hyperparameter values displayed in Table 2 are obtained by using the grid search capability from the Python machine learning library, `scikit-learn` (Pedregosa et al., 2011). The validation set used for tuning the hyperparameters is as described in Section 2. During training, we input the training sample at each time point in the training set into the model to train the model. When training is complete, the neuron weights in the model are optimized. During testing, we input the test sample at each time point in the test set into the trained model and calculate the model's prediction accuracy. Training and test samples are also as described in Section 2. The training, validation and testing processes were run and completed on an NVIDIA A100 GPU.

It should be pointed out that although both our SINet and the existing TimesNet (Wu et al., 2023) adopt TimesBlocks, they differ in several ways. First, TimesNet employs five most significant period components in a TimesBlock, while SINet uses three most significant period components to reduce model complexity. Second, TimesNet uses SMAPE as the loss function and a batch size of 16. In contrast, SINet uses MSE as the loss function and a batch size of 32. In our case, the SMAPE loss function performs worse than MSE. Third, TimesNet is mainly designed for multivariate time series forecasting and employs a model dimension of 32. In contrast, SINet is

Table 2
Model Training Conditions of SINet

Loss function	Optimizer	Learning rate	Dropout rate	Batch size	Epoch
MSE	Adam	0.001	0.3	32	10

designed for univariate time series forecasting specifically for F10.7 and F30 predictions, and adopts a model dimension of 64, which is more suitable for our work. In contrast to other time series forecasting methods such as long short-term memory (LSTM; Hochreiter & Schmidhuber, 1997; Zhu et al., 2022) and temporal convolutional network (TCN; Wang et al., 2024), which process the input time series data directly, SINet converts the input data from the time domain to the frequency domain through a FFT algorithm to enhance learning effectiveness.

4. Results

4.1. Evaluation Metrics

We employ two different approaches with SINet: fixed prediction, denoted SINet_f, and rolling prediction, denoted SINet_r, as explained in Section 2. We adopt three metrics to evaluate the performance of the two approaches and related methods. The three metrics are the root mean square error (RMSE), the mean absolute error (MAE), and the mean absolute percentage error (MAPE; Myttenaere et al., 2016).

Let N be the number of test samples. For each test sample, we used the historical values of F10.7 (F30, respectively) of the previous 30 days to predict the values of F10.7 (F30, respectively) in the future. We focus on the k-day ahead prediction for $k = 1, 27, 45, 60$, respectively. Let $\hat{y}_i$, $1 \le i \le N$, denote a predicted value, and let y_i denote the corresponding observed/true value. RMSE is calculated as:

$$\text{RMSE} = \sqrt{\frac{1}{N}\sum_{i=1}^{N}(\hat{y}_i - y_i)^2}. \tag{2}$$

MAE is calculated as:

$$\text{MAE} = \frac{1}{N}\sum_{i=1}^{N}|\hat{y}_i - y_i|. \tag{3}$$

MAPE is calculated as:

$$\text{MAPE} = \frac{1}{N}\sum_{i=1}^{N}\frac{|\hat{y}_i - y_i|}{y_i} \times 100\%. \tag{4}$$

The units of RMSE and MAE are sfu while the unit of MAPE is percentage. The smaller the RMSE, MAE and MAPE are, the better a method performs. As in Jiang et al. (2025), we use MAPE as the primary metric.

4.2. Experimental Results for F10.7

4.2.1. Performance Evaluation of SINet on F10.7 Prediction

We calculated the performance metric values of SINet_f and SINet_r, and compared the metric values with those of five closely related forecasting methods for F10.7. The five methods include autoregressive integrated moving average (ARIMA; Box & Jenkins, 1970), long short-term memory (LSTM; Hochreiter & Schmidhuber, 1997; Zhu et al., 2022), convolutional neural network (CNN; LeCun et al., 1998), LSTM with multihead attention (LSTM+; Vaswani et al., 2017; Jerse & Marcucci, 2024), and temporal convolutional network (TCN; Wang et al., 2024). Among the five methods, ARIMA is a statistical learning method, while the other four are based on deep learning models.

To increase the reliability of model evaluation, we conduct a 5-fold validation experiment. To prevent data leakage and preserve the temporal order of the data, the training set and test set in the 5-fold experiment are constructed as follows. In fold 1, the training set and test set are as shown in Figure 1. In fold i, $2 \le i \le 5$, we remove the first $i - 1$ months of data from the training set in fold 1 to get a new training set for fold i, and remove the last $i - 1$ months of data from the test set in fold 1 to get a new test set for fold i. Thus, for fold i and fold j, where $i \ne j$, the training data and the test data in fold i differ from the training data and the test data in fold j. In each fold, we use the training data in that fold to train a model and then use the test data in that fold to test the trained model, to calculate the metric values in the fold. Table 3 presents the average and standard deviation of MAPE

Table 3
Average and Standard Deviation of Mean Absolute Percentage Error (%) Obtained by SINet and Related Methods on F10.7 Prediction in the 5-Fold Validation Experiment

Forecast	$SINet_f$	$SINet_r$	ARIMA	LSTM	CNN	LSTM+	TCN
1st Day	**2.3** ± 0.1	**2.3** ± 0.1	2.4 ± 0.0	2.8 ± 0.1	3.0 ± 0.2	2.5 ± 0.1	2.4 ± 0.1
27th Day	**8.0** ± 0.1	8.8 ± 0.2	9.1 ± 0.1	8.9 ± 0.2	8.5 ± 0.2	8.7 ± 0.1	8.6 ± 0.1
45th Day	**9.1** ± 0.1	9.3 ± 0.1	11.3 ± 0.1	11.0 ± 0.4	9.6 ± 0.1	9.6 ± 0.2	9.4 ± 0.1
60th Day	**10.1** ± 0.1	10.9 ± 0.3	11.6 ± 0.0	11.1 ± 0.5	10.7 ± 0.5	10.4 ± 0.1	10.4 ± 0.3

over the five folds (more detailed results can be found in Appendix A). The best (lowest) average MAPE for each forecast horizon is highlighted in boldface. It can be seen from Table 3 that $SINet_f$ performs better than the other methods, demonstrating its strong capability in capturing the temporal dynamics of solar flux variability. TCN is generally the second best method. For the 1-day ahead prediction, $SINet_f$ and $SINet_r$ are identical methods. For the larger forecast horizons, $SINet_f$ outperforms $SINet_r$, indicating the advantage of the fixed prediction approach over the rolling prediction approach. Results of the other metrics are similar and omitted.

4.2.2. Further Assessment of SINet and TCN on F10.7 Prediction

We further compared the proposed approaches with the TCN method on the 60-day ahead prediction of F10.7 in the period between 2009 and 2021. The training set and test set are as shown in Figure 1, which are the same as those used in fold 1 in Table A4. Figure 4 presents the annual comparison results and the overall comparison results of the three methods. It can be seen in Figure 4 that the fixed prediction approach, $SINet_f$, performs better than TCN and the rolling prediction approach, $SINet_r$, in the overall comparison results, which are consistent with the results reported in Section 4.2.1. Specifically, $SINet_f$ achieves the lowest RMSE of 16.32 sfu, MAE of 10.92 sfu, and MAPE of 10.2%, compared to RMSE of 17.19 sfu, MAE of 11.53 sfu, and MAPE of 10.8% (RMSE of 17.14 sfu, MAE of 11.31 sfu, and MAPE of 10.4%, respectively) obtained by TCN ($SINet_r$, respectively). $SINet_f$ improves TCN by 5.06% in RMSE, 5.29% in MAE, and 5.56% in MAPE. As pointed out in Subsection 4.2.1, the rolling prediction approach is worse than the fixed prediction approach. This happens probably because, during the rolling, the historical values of the previous 30 days used to predict the 60-day ahead F10.7 value are all synthetic F10.7 values rather than true F10.7 values.

We note that in the solar maximum (i.e., 2014) the three methods studied here are less accurate, and our proposed $SINet_f$ is much better than TCN in this period. Figure 5 provides a detailed comparison of the three methods for daily predictions of F10.7 in 2014. It can be seen in Figure 5 that $SINet_f$ (TCN, $SINet_r$, respectively) achieves an RMSE of 26.52 sfu (31.25 sfu, 31.09 sfu, respectively), an MAE of 20.94 sfu (24.19 sfu, 24.38 sfu, respectively), and an MAPE of 14.5% (15.9%, 16.4%, respectively) in 2014. $SINet_f$ improves TCN by 15.14% in RMSE, 13.44% in MAE, and 8.81% in MAPE in 2014. There is a significant improvement of $SINet_f$ over TCN in the solar maximum.

Figure 6 compares the observed/true values and the $SINet_f$-predicted F10.7 values with four forecast horizons: 1, 27, 45 and 60 days, respectively, in the period between 2009 and 2021. Each dashed blue line represents the observed F10.7 values, while each solid black line represents the synthetic F10.7 values predicted by $SINet_f$. In general, the $SINet_f$ method is able to capture the trend of F10.7. However, the larger the forecast horizon, the less accurate $SINet_f$ is. For 1-day ahead forecasts, $SINet_f$ achieves an RMSE of 3.88 sfu, an MAE of 2.38 sfu, and an MAPE of 2.2%. For 60-day ahead forecasts, $SINet_f$ achieves an RMSE of 16.32 sfu, MAE of 10.92 sfu, and MAPE of 10.2%. The results of 60-day ahead forecasts are worse than those of 1-day ahead forecasts.

Recently, K. Zhang et al. (2024) used a deep learning method, called Informer, to make daily predictions of F10.7 (1–27 days in advance). When comparing $SINet_f$ with the Informer model in the solar maximum (i.e., 2014), the mean of RMSE, MAE, and MAPE, averaged over 1–27 forecast horizons, for the Informer model is 23 sfu, 18 sfu, and 13%, respectively. The mean of RMSE, MAE, and MAPE, averaged over 1–27 forecast horizons, for our $SINet_f$ method is 22 sfu, 17 sfu, and 11%, respectively. When comparing the mean values of annual average forecast errors with 1–27 forecast horizons in the period between 2017 and 2021, Informer achieves an RMSE of 6.285 sfu, an MAE of 3.789 sfu, and an MAPE of 4.54%. $SINet_f$ achieves an RMSE of 5.881 sfu, an MAE of 3.843 sfu, and an MAPE of 4.53%. Although the Informer model and $SINet_f$ use different prediction techniques

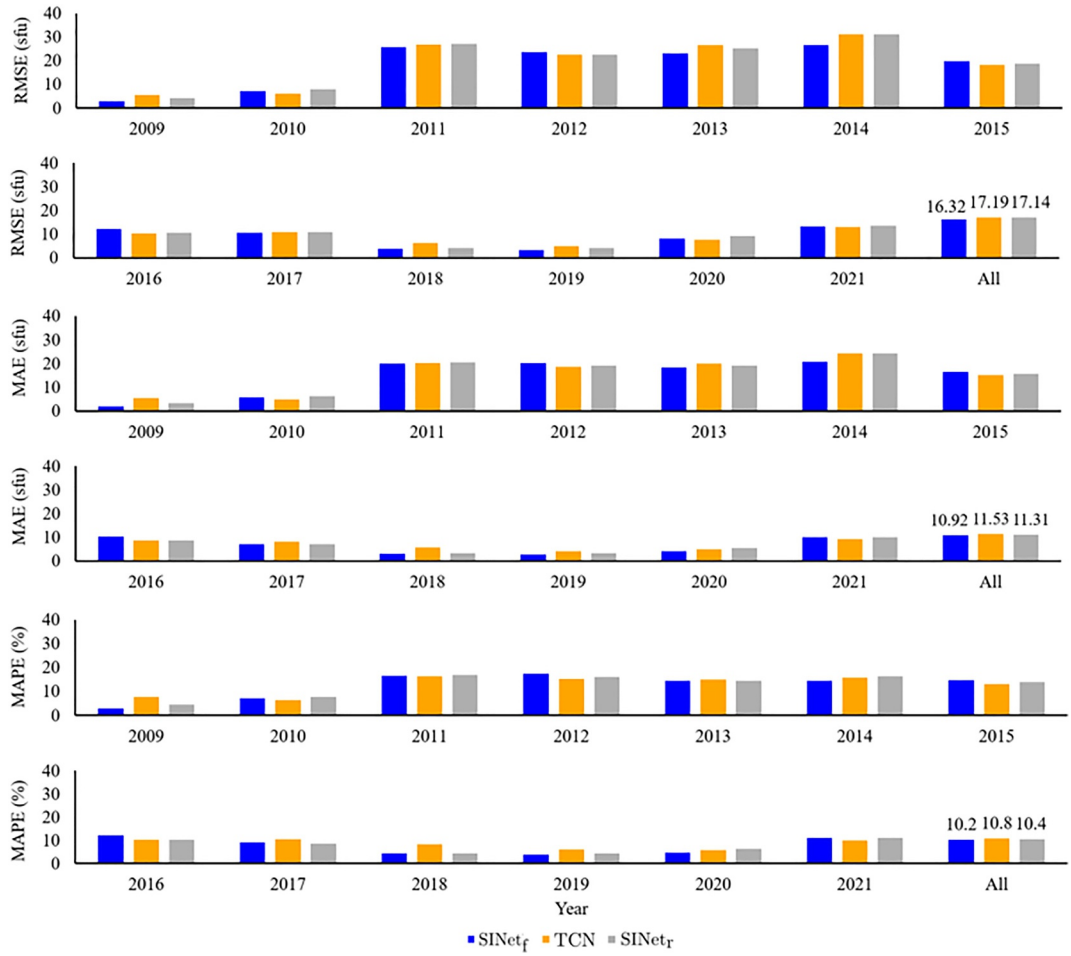

Figure 4. Comparison of three forecasting methods: $SINet_f$, temporal convolutional network and $SINet_r$, on the 60-day ahead prediction of F10.7 in the period between 2009 and 2021. The figure shows the annual comparison results and the overall comparison results in this period.

with different training and test data, these performance metric values indicate that our proposed approach is comparable to the Informer model in making daily predictions of F10.7 for 1–27 forecast horizons.

4.3. Experimental Results for F30

4.3.1. Performance Evaluation of SINet on F30 Prediction

Here, we calculated the performance metric values of $SINet_f$ and $SINet_r$ and compared the metric values with those of the five closely related forecasting methods (ARIMA, LSTM, CNN, LSTM+, TCN) for F30 using the 5-fold validation experiment as described in Section 4.2.1. Table 4 presents the average and standard deviation of MAPE over the five folds (more detailed results can be found in Appendix A). The best (lowest) average MAPE for each forecast horizon is highlighted in boldface. Again, Table 4 shows that $SINet_f$ is the best method while TCN is generally the second best method in terms of MAPE. Results of the other metrics are similar and omitted.

4.3.2. Further Assessment of SINet and TCN on F30 Prediction

We further compared the proposed approaches with the TCN method on the 60-day ahead prediction of F30 in the period between 2009 and 2021. The training set and test set are as shown in Figure 1, which are the same as those used in fold 1 in Table A8. Figure 7 presents the annual comparison results and the overall comparison results of the three methods. As in the F10.7 case, $SINet_f$ performs the best in the overall comparison results on F30 prediction. $SINet_f$ achieves an RMSE of 9.99 sfu, MAE of 6.81 sfu, and MAPE of 9.5%, compared to the RMSE

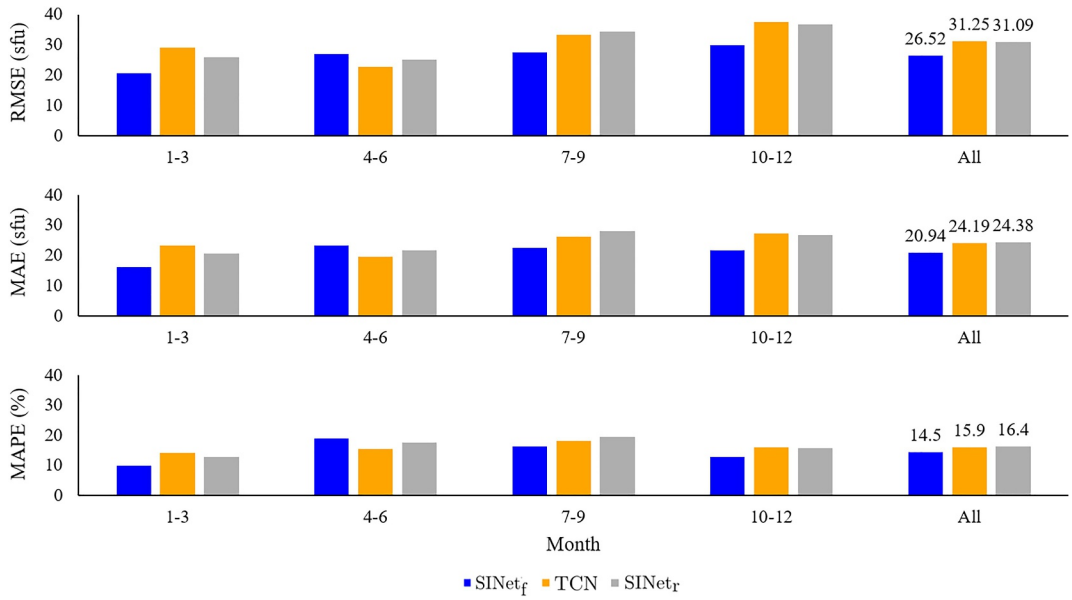

Figure 5. Comparison of three forecasting methods: $SINet_f$, temporal convolutional network and $SINet_r$, on the 60-day ahead prediction of F10.7 in the solar maximum (2014). The figure shows the quarterly comparison results and the overall comparison results in 2014.

of 10.55 sfu, MAE of 7.03 sfu, and MAPE of 9.6% (RMSE of 10.17 sfu, MAE of 6.93 sfu, and MAPE of 9.6%, respectively) obtained by TCN ($SINet_r$, respectively). $SINet_f$ improves TCN by 5.31% in RMSE, 3.13% in MAE, and 1.04% in MAPE. Comparing Figure 7 with Figure 4, we see that $SINet_f$ achieves higher accuracy in F30 than in F10.7. This happens because, in the test set, the range of the F30 values, which are 38.9 sfu to 199.1 sfu, is much smaller than the range of the F10.7 values, which are 65.7 sfu to 371.1 sfu. A smaller range with lower variability causes smaller prediction errors.

Again, we note that in the solar maximum (i.e., 2014) the three methods studied here are less accurate, and our proposed $SINet_f$ is much better than TCN in this period. Figure 8 provides a detailed comparison of the three methods for daily predictions of F30 in 2014. It can be seen in Figure 8 that $SINet_f$ (TCN, $SINet_r$, respectively) achieves an RMSE of 14.53 sfu (19.32 sfu, 15.39 sfu, respectively), an MAE of 11.23 sfu (15.72 sfu, 11.80 sfu, respectively), an MAPE of 11.0% (14.7%, 11.6%, respectively). $SINet_f$ improves TCN by 24.79% in RMSE, 28.56% in MAE, and 25.17% in MAPE. Again, there is a significant improvement of $SINet_f$ over TCN in the solar maximum.

Figure 9 compares the observed/true values and the $SINet_f$-predicted F30 values with four forecast horizons: 1, 27, 45, and 60 days, respectively, in the period between 2009 and 2021. Each dashed blue line represents the observed F30 values, while each solid black line represents the synthetic F30 values predicted by $SINet_f$. Like the F10.7 case, the $SINet_f$ method is able to capture the trend of F30. However, the larger the forecast horizon, the less accurate $SINet_f$ is. For 1-day ahead forecasts, $SINet_f$ achieves an RMSE of 2.05 sfu, an MAE of 1.40 sfu, and an MAPE of 2.0%. For 60-day ahead forecasts, $SINet_f$ achieves an RMSE of 9.99 sfu, MAE of 6.81 sfu, and MAPE of 9.5%. Comparing Figure 9 with Figure 6, we see that the predicted values of F30 are closer to the observed/true values than those of F10.7.

4.4. Daily Predictions During the Period of Active Region NOAA 12673

Active Region (AR) NOAA 12673 was most active in September 2017, specifically between 4 September 2017 and 10 September 2017. It was a super-flaring AR that produced numerous solar flares, including a very large X9.3 flare. This region showed exceptionally fast magnetic flux emergence and was characterized by a complex interplay of magnetic field and dynamics. One wonders how the $SINet_f$ method performs during the very dynamic AR 12673 period.

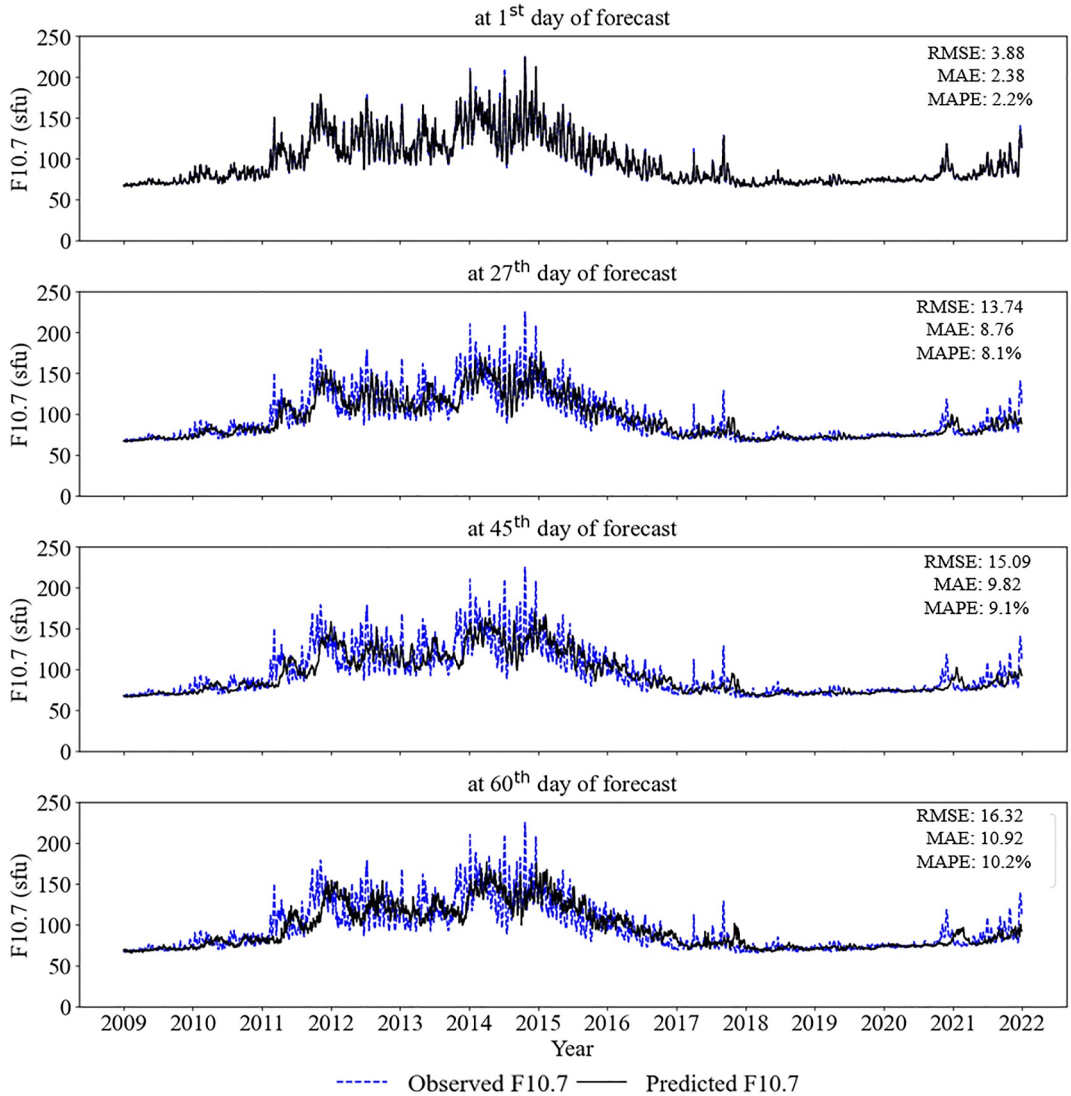

Figure 6. Daily predictions of the F10.7 solar index made by our $SINet_f$ method with four forecast horizons: 1, 27, 45, and 60 days, respectively, in the period between 2009 and 2021.

Our trained $SINet_f$ model was fed with solar index values in the period between 2 August 2017 and 31 August 2017 and made daily predictions of F10.7 and F30 in the period between 1 September 2017 and 30 October 2017 (1–60 days in advance). Figure 10 shows the results, in which the prediction error on a day is defined as the absolute value of the difference between the true/observed value and the $SINet_f$-predicted value on that day. The solid blue line represents the prediction errors for F10.7 and the dotted red line represents the prediction errors for

Table 4
Average and Standard Deviation of Mean Absolute Percentage Error (%) Obtained by SINet and Related Methods on F30 Prediction in the 5-Fold Validation Experiment

Forecast	$SINet_f$	$SINet_r$	ARIMA	LSTM	CNN	LSTM+	TCN
1st Day	**2.0** ± 0.0	**2.0** ± 0.0	2.1 ± 0.0	2.6 ± 0.2	3.4 ± 0.2	2.4 ± 0.2	2.4 ± 0.2
27th Day	**7.1** ± 0.1	7.9 ± 0.1	7.6 ± 0.1	8.5 ± 0.1	8.2 ± 0.1	7.6 ± 0.1	7.5 ± 0.2
45th Day	**8.7** ± 0.1	8.9 ± 0.2	10.5 ± 0.1	10.6 ± 0.1	9.0 ± 0.3	9.9 ± 0.2	9.2 ± 0.3
60th Day	**9.5** ± 0.1	10.2 ± 0.3	10.7 ± 0.0	10.3 ± 0.1	10.2 ± 0.1	9.6 ± 0.1	9.6 ± 0.1

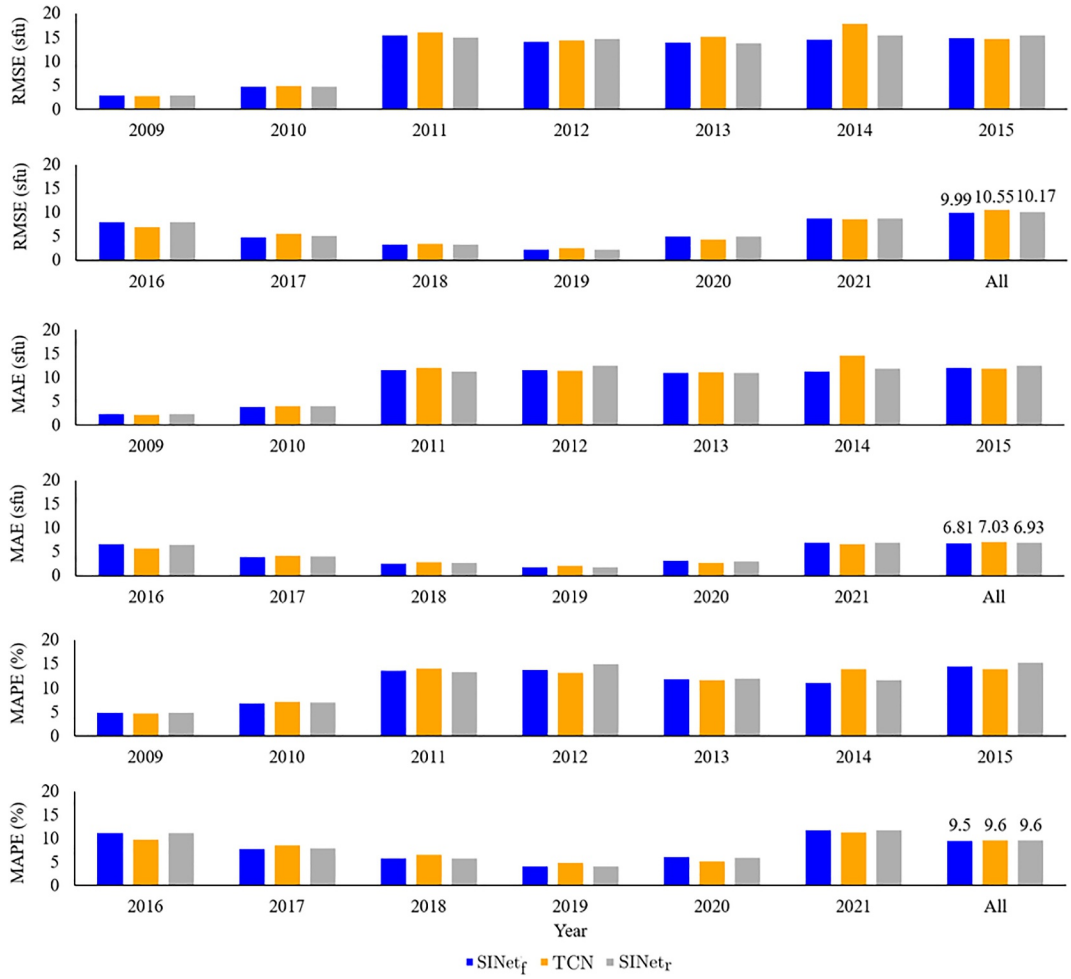

Figure 7. Comparison of three forecasting methods: $SINet_f$, temporal convolutional network and $SINet_r$, on the 60-day ahead prediction of F30 in the period between 2009 and 2021. The figure shows the annual comparison results and the overall comparison results in this period.

F30. It can be seen in Figure 10 that the prediction errors are higher in the period between 4 September 2017 and 10 September 2017 (i.e., between day 4 and day 10 on the *X*-axis) than in the other periods. This happens probably because there are relatively few training samples related to such a fast magnetic flux emergence as in the dynamic AR 12673 period, and hence its pattern is not captured by the $SINet_f$ model during training. Consequently, during testing/prediction, the pattern can not be recognized, and hence the model does not perform well in this period.

This case study shows that our $SINet_f$ model suffers when encountering the emergence of new, very active ARs where the AR emergence is much more a random process than the AR decay process. This is a limitation of all solar activity forecasting models. Overcoming this limitation can be challenging. Literature suggests several ways to alleviate this challenging problem, which include removing solar transient events such as very large flares and coronal mass ejections from the data set (Jiang et al., 2025), or using oversampling (Jiang et al., 2025) and data augmentation techniques (H. Zhang et al., 2025) to increase model's knowledge of the most active ARs. Another possible way is to create a separate machine learning model, such as an anomaly prediction model (Fahim & Sillitti, 2019), dedicated to solar index forecasting during solar transient events.

5. Discussion

The input length of our $SINet_f$ model is 30 days, which is approximately a solar rotation period (see Figure 2). It is known that solar variability can be characterized with a 7-month long impulse function; specifically, after an AR emerges, its impact on solar irradiance decays over 7 solar rotations (e.g., Dudok de Wit et al., 2018; Preminger &

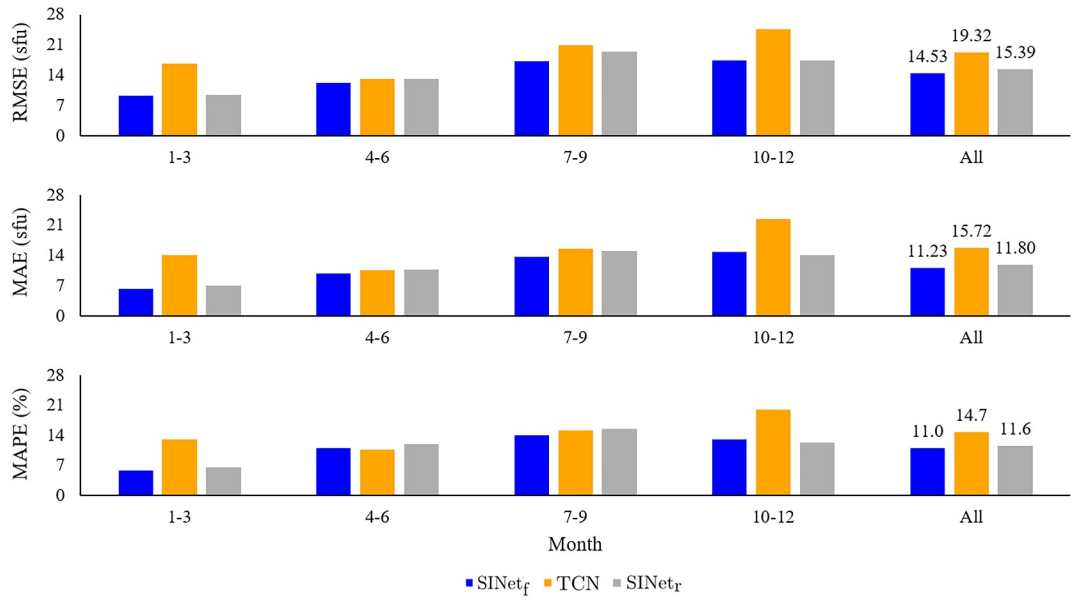

Figure 8. Comparison of three forecasting methods: SINet$_f$, temporal convolutional network and SINet$_r$, on the 60-day ahead prediction of F30 in the solar maximum (2014). The figure shows the quarterly comparison results and the overall comparison results in 2014.

Walton, 2005). It is worthwhile to consider using more than 1-month data for the model input so that our model might do better at capturing the known solar physical effect of AR impacts on solar irradiance variability. We conducted additional experiments to evaluate the impact of the input length on model performance. It was found that using input data of more months (e.g., 2-month, 3-month, 4-month, etc.) produced similar results, though model training time increased substantially. Information in one solar rotation period suffices for the model to make decisions on solar irradiance predictions. Similarly, we selected the 3 most significant periodic components when using the FFT algorithm to convert the input data from the time domain to the frequency domain (see Figure 3). Increasing the number of components produced similar results while increasing model training time. On the other hand, selecting too few components (e.g., 1 or 2 components) led to worse performance.

Figures 4 and 7 show that our SINet$_f$ model has the best metrics averaged over the 13 years from 2009 to 2021, but is worse than the state-of-the-art TCN model in some individual years (e.g., 2016). This happens probably because TCN is designed to capture temporal patterns in time series. In 2016, TCN can better capture such patterns in solar index time series with less variability when solar activity is weaker. However, in the solar maximum (2014) or in the solar minimum (2019) during which such temporal patterns do not exist, SINet$_f$ shows better inference capability and achieves better performance than TCN.

Figures 6 and 9 show that SINet$_f$ has an autocorrelation basis; specifically, past solar rotation is largely duplicated into the forecast. We investigated this autocorrelation effect by considering predictions with a forecast horizon of 1 day since these predictions are most accurate. Mathematically, the autocorrelation at lag k, denoted $\hat{\rho}_k$, is defined as

$$\hat{\rho}_k = \frac{\sum_{t=k+1}^{N}\left(\hat{y}_t - \overline{\hat{y}}\right)\left(\hat{y}_{t-k} - \overline{\hat{y}}\right)}{\sum_{t=1}^{N}\left(\hat{y}_t - \overline{\hat{y}}\right)^2}, \quad k = 1, 27, 45, 60, \tag{5}$$

where $\hat{y}_t$ denotes the predicted value at time point t, $\overline{\hat{y}}$ is the mean of the predicted series, and N is the total number of time points. The statistic $\hat{\rho}_k$ measures the autocorrelation between the predicted value $\hat{y}_t$ and its k-day lagged version $\hat{y}_{t-k}$.

Figure 11 (Figure 12, respectively) presents results for F10.7 (F30, respectively). It can be seen from the figures that there is a clear autocorrelation effect at lag 1 for all the seven methods studied here. This result is understandable given that the one-day ahead prediction is highly accurate, as shown in Sections 4.2.1 and 4.3.1, and

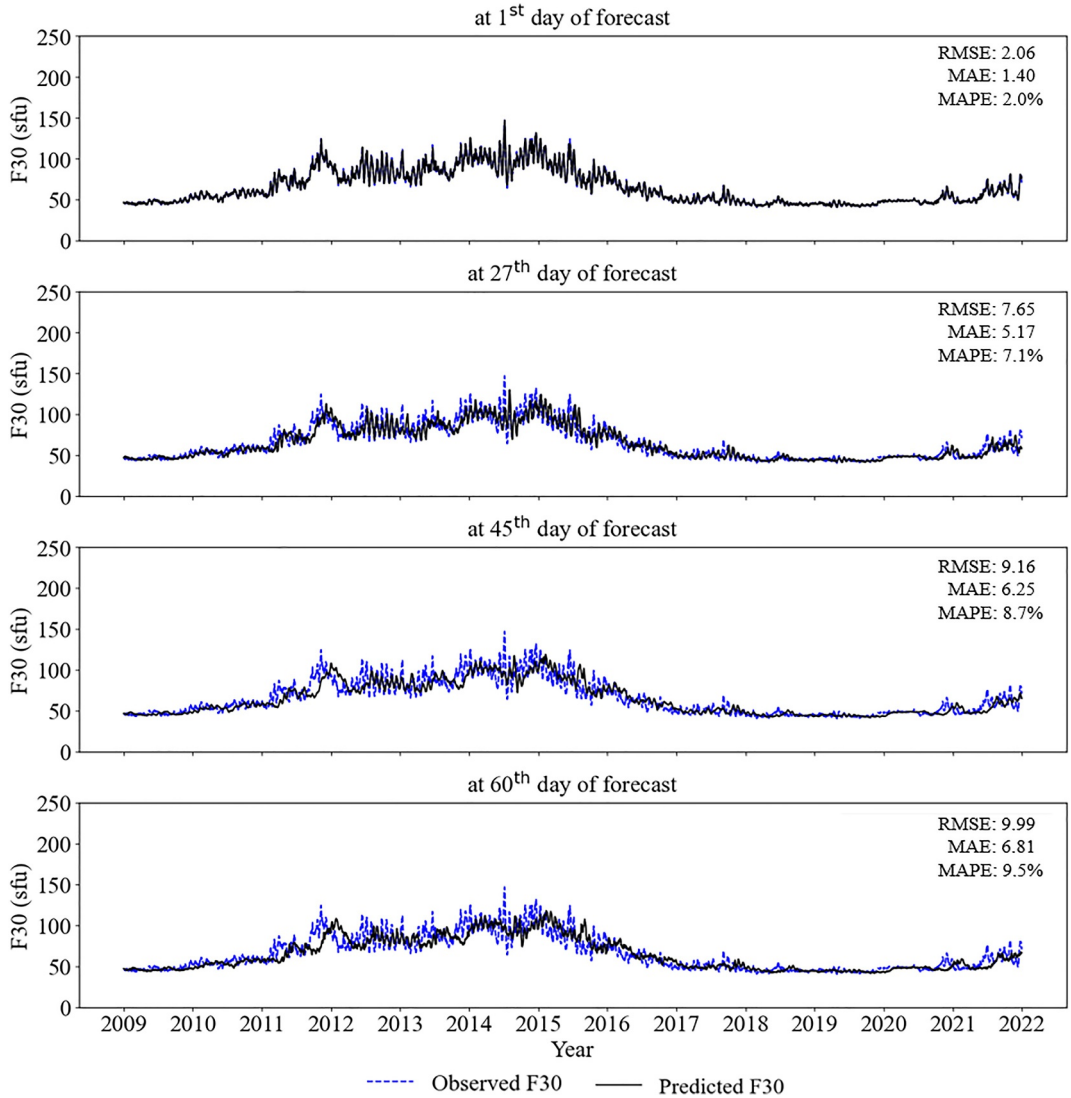

Figure 9. Daily predictions of the F30 solar index made by our $SINet_f$ method with four forecast horizons: 1, 27, 45, and 60 days, respectively, in the period between 2009 and 2021.

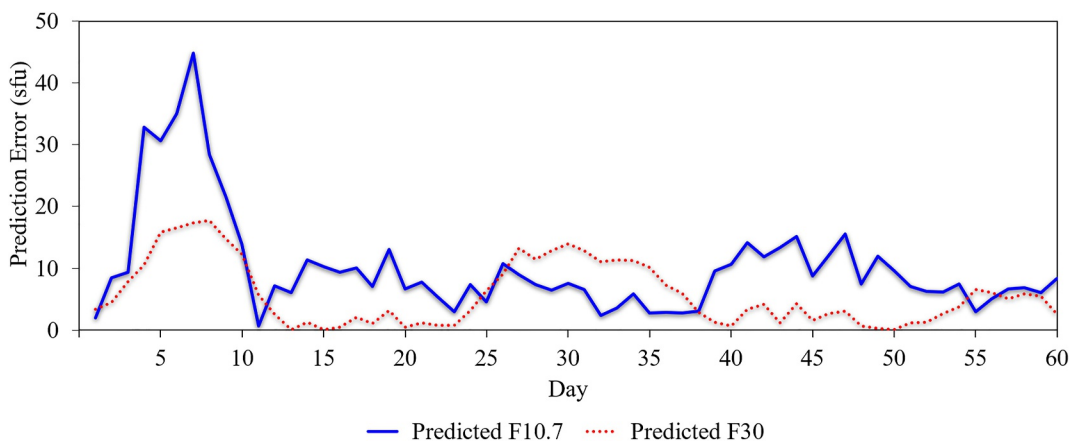

Figure 10. Prediction errors made by $SINet_f$ for the F10.7 and F30 solar indices in the period between 1 September 2017 and 30 October 2017 (i.e., between day 1 and day 60 on the *X*-axis).

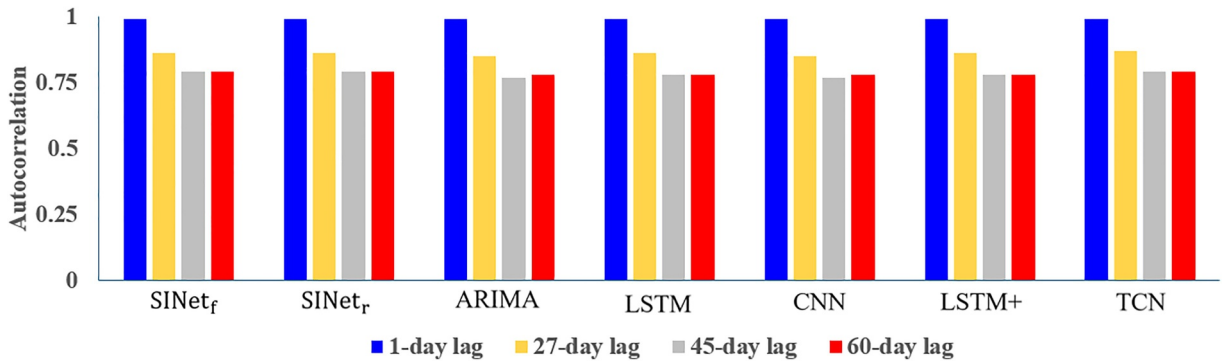

Figure 11. Comparison of autocorrelation effects among seven forecasting methods on the 1-day ahead prediction of F10.7 in the period between 2009 and 2021.

there is not much change in solar irradiance within one day. In contrast, when k is larger, the autocorrelation effect is less evident, suggesting that the predicted values are less autocorrelated over a longer period, as solar activity may vary in the period.

6. Conclusion

In this study, we presented a novel deep learning model (SINet) for making medium-term daily predictions of the F10.7 and F30 solar indices (1–60 days in advance). SINet is an enhancement of TimesNet (Wu et al., 2023), specifically designed to capture short- and long-range dependencies in the time series of F10.7 and F30 values. The model takes advantage of the frequency domain decomposition via a FFT algorithm with a dual-inception model structure, enabling effective extraction of dominant periodic components in the time series data.

We adopted fixed and rolling prediction approaches, denoted SINet$_f$ and SINet$_r$, respectively, and compared them with five closely related statistical and deep learning methods (ARIMA, LSTM, CNN, LSTM+, TCN). Extensive experiments show that SINet$_f$ performs the best while TCN is generally the second best method. When predicting the F10.7 solar index (60 days in advance), TCN achieves an RMSE of 17.19 sfu, MAE of 11.53 sfu, and MAPE of 10.8%, in the period between 2009 and 2021. In contrast, SINet$_f$ achieves an RMSE of 16.32 sfu, MAE of 10.92 sfu, and MAPE of 10.2%, in the same period. When predicting the F30 solar index (60 days in advance), TCN achieves an RMSE of 10.55 sfu, MAE of 7.03 sfu, and MAPE of 9.6%, in this period. In contrast, SINet$_f$ achieves an RMSE 9.99 sfu, MAE of 6.81 sfu, and MAPE of 9.5%, in the period. In the solar maximum (2014), TCN achieves an RMSE of 31.25 sfu, MAE of 24.19 sfu, and MAPE of 15.9% for F10.7 and an RMSE of 19.32 sfu, MAE of 15.72 sfu, and MAPE of 14.7% for F30. In contrast, SINet$_f$ achieves an RMSE of 26.52 sfu, MAE of 20.94 sfu, and MAPE of 14.5% for F10.7 and an RMSE of 14.53 sfu, MAE of 11.23 sfu, and MAPE of 11.0% for F30. SINet$_f$ improves the state-of-the-art TCN method significantly during the solar maximum for 60-day ahead forecasts. Based on these results, we conclude that SINet$_f$ is a feasible model to make medium-term daily predictions of the F10.7 and F30 solar indices.

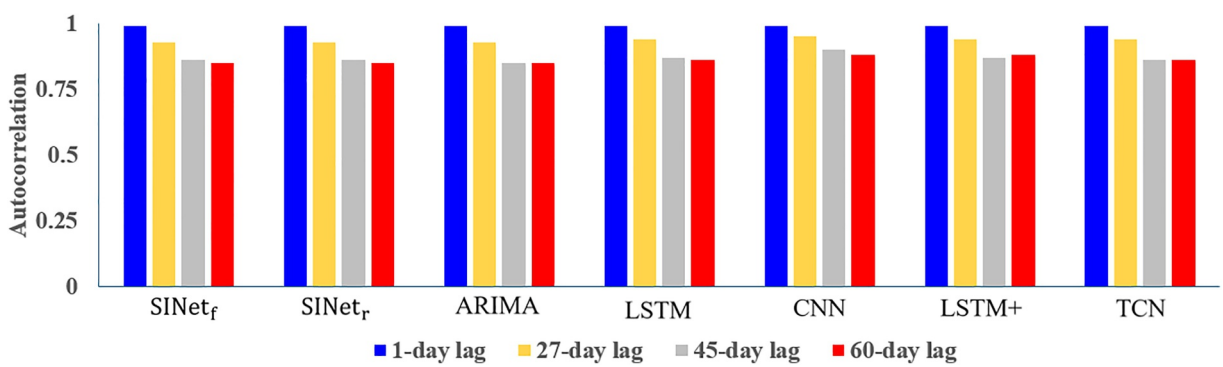

Figure 12. Comparison of autocorrelation effects among seven forecasting methods on the 1-day ahead prediction of F30 in the period between 2009 and 2021.

We have implemented $SINet_f$ into an operational F10.7 forecasting system. Visit https://nature.njit.edu/solardb/, click the "Tools" tab and select "F10.7 Forecasting" in the drop-down menu to access the $SINet_f$ system. The NOAA Space Weather Prediction Center (SWPC) also provides an operational F10.7 forecasting system, which produces 45-day forecasts of F10.7 at https://www.swpc.noaa.gov/products/usaf-45-day-ap-and-f107cm-flux-forecast (Warren et al., 2017). We compared our $SINet_f$ system with the NOAA/SWPC forecasting system in the period between 29 March 2025 and 24 June 2025, during which observed F10.7 values and archived F10.7 predictions at NOAA/SWPC are available. It was found that, on the operational F10.7 predictions, the MAPE of the $SINet_f$ system is 13.8%, which is slightly better than the MAPE of 14.0% achieved by the NOAA/SWPC forecasting system, suggesting that our $SINet_f$ system can complement the existing NOAA/SWPC forecasting system.

Appendix A: Detailed 5-Fold Validation Results for F10.7 and F30

Table A1 (Table A2, Table A3, and Table A4, respectively) presents MAPE results of an F10.7 forecasting method obtained in each fold of the 5-fold validation experiment at the 1st day of forecast (the 27th day of forecast, the 45th day of forecast, and the 60th day of forecast, respectively). Table A5 (Table A6, Table A7, and Table A8, respectively) presents MAPE results of an F30 forecasting method obtained in each fold of the 5-fold validation experiment at the 1st day of forecast (the 27th day of forecast, the 45th day of forecast, and the 60th day of forecast, respectively). The best (lowest) MAPE value for each fold is highlighted in boldface. Each MAPE value of a forecasting method is associated with a *p*-value obtained by applying the Wilcoxon signed-rank test (Wilcoxon, 1945) to the forecasting method and $SINet_f$, where a *p*-value less than or equal to 0.05 indicates a statistically significant result. For the 1-day ahead prediction, $SINet_f$ and $SINet_r$ are identical methods.

Table A1
Mean Absolute Percentage Error (%) of SINet and Related Methods on F10.7 Prediction (at 1st Day of Forecast)

	$SINet_f$	$SINet_r$	ARIMA	LSTM	CNN	LSTM+	TCN
Fold 1	**2.2**	**2.2**	2.4	2.8	2.4	2.4	2.3
p-value		—	2.9E−2	8.3E−70	1.3E−31	7.1E−26	1.7E−39
Fold 2	**2.3**	**2.3**	2.4	3.1	2.4	2.6	2.4
p-value		—	9.5E−2	1.5E−83	9.6E−10	1.7E−62	5.9E−15
Fold 3	**2.3**	**2.3**	2.4	2.6	2.8	2.6	2.4
p-value		—	1.3E−1	2.3E−50	1.9E−90	7.8E−47	3.9E−16
Fold 4	**2.2**	**2.2**	2.4	3.1	2.8	2.4	2.4
p-value		—	8.1E−2	9.8E−51	1.1E−93	1.1E−13	1.7E−31
Fold 5	**2.2**	**2.2**	2.4	3.1	2.8	2.4	2.4
p-value		—	1.4E−2	7.1E−112	3.7E−139	5.5E−27	3.1E−46

Table A2
Mean Absolute Percentage Error (%) of SINet and Related Methods on F10.7 Prediction (at 27th Day of Forecast)

	$SINet_f$	$SINet_r$	ARIMA	LSTM	CNN	LSTM+	TCN
Fold 1	**8.1**	8.7	9.2	8.7	8.7	8.8	8.7
p-value		4.6E−25	2.8E−10	2.7E−15	9.8E−30	1.8E−51	7.7E−105
Fold 2	**8.0**	8.8	9.1	8.8	8.5	8.7	8.7
p-value		1.6E−23	1.6E−11	3.8E−19	2.4E−44	7.7E−27	3.1E−21
Fold 3	**8.1**	9.0	9.1	8.9	8.4	8.8	8.5
p-value		2.6E−18	1.5E−9	1.8E−18	3.5E−24	1.1E−69	4.9E−55

Table A2
Continued

	$SINet_f$	$SINet_r$	ARIMA	LSTM	CNN	LSTM+	TCN
Fold 4	**8.0**	8.6	9.1	9.2	8.3	8.7	8.6
p-value		5.2E−17	2.7E−10	7.9E−31	2.7E−20	6.7E−24	6.7E−31
Fold 5	**8.0**	9.0	9.1	9.1	8.6	8.7	8.5
p-value		3.0E−28	8.3E−12	5.0E−63	6.3E−25	1.4E−20	1.1E−54

Table A3
Mean Absolute Percentage Error (%) of SINet and Related Methods on F10.7 Prediction (at 45th Day of Forecast)

	$SINet_f$	$SINet_r$	ARIMA	LSTM	CNN	LSTM+	TCN
Fold 1	**9.1**	9.2	11.4	11.3	9.7	9.8	9.4
p-value		1.4E−1	5.5E−16	3.7E−207	1.5E−10	3.7E−70	8.1E−45
Fold 2	**9.1**	9.3	11.3	10.7	9.7	9.3	9.3
p-value		8.3E−1	2.2E−18	2.4E−142	1.7E−7	1.1E−83	1.7E−36
Fold 3	**9.2**	9.3	11.3	11.3	9.7	9.5	9.4
p-value		4.7E−3	2.6E−16	2.4E−175	1.1E−17	1.3E−154	3.7E−50
Fold 4	**9.2**	9.3	11.3	11.3	9.6	9.5	9.5
p-value		6.5E−1	1.1E−16	1.8E−183	4.4E−6	1.9E−57	1.5E−11
Fold 5	**9.2**	9.4	11.3	10.5	9.6	9.7	9.3
p-value		3.1E−11	4.8E−16	2.6E−263	2.9E−7	3.8E−138	7.6E−2

Table A4
Mean Absolute Percentage Error (%) of SINet and Related Methods on F10.7 Prediction (at 60th Day of Forecast)

	$SINet_f$	$SINet_r$	ARIMA	LSTM	CNN	LSTM+	TCN
Fold 1	**10.2**	10.4	11.6	10.6	11.6	10.6	10.8
p-value		2.3E−13	6.9E−10	1.9E−48	1.1E−7	4.8E−13	5.0E−7
Fold 2	**10.0**	10.7	11.6	10.8	10.5	10.6	10.5
p-value		7.9E−5	1.1E−10	2.9E−111	9.8E−9	8.1E−10	1.5E−32
Fold 3	10.1	11.0	11.6	10.9	10.6	10.4	**10.0**
p-value		1.3E−11	1.0E−10	2.7E−71	3.3E−8	4.6E−8	1.0E−11
Fold 4	**10.1**	10.6	11.6	11.7	10.4	10.4	10.3
p-value		9.2E−6	6.2E−9	2.0E−7	1.4E−4	1.9E−22	4.4E−8
Fold 5	**10.1**	11.3	11.6	11.7	10.4	10.4	10.4
p-value		1.7E−18	1.4E−10	1.0E−48	7.7E−12	4.5E−5	9.6E−12

Table A5
Mean Absolute Percentage Error (%) of SINet and Related Methods on F30 Prediction (at 1st Day of Forecast)

	$SINet_f$	$SINet_r$	ARIMA	LSTM	CNN	LSTM+	TCN
Fold 1	**2.0**	**2.0**	2.1	2.4	3.7	2.1	2.2
p-value		—	1.2E−2	2.0E−78	1.9E−299	7.8E−26	1.6E−44
Fold 2	**2.0**	**2.0**	2.1	2.7	3.3	2.2	2.7
p-value		—	1.1E−1	2.7E−127	3.4E−235	2.5E−23	2.9E−146

Table A5
Continued

	$SINet_f$	$SINet_r$	ARIMA	LSTM	CNN	LSTM+	TCN
Fold 3	**2.0**	**2.0**	2.1	2.7	3.4	2.5	2.1
p-value		—	2.5E−2	1.0E−149	1.1E−279	1.0E−96	5.9E−23
Fold 4	**2.0**	**2.0**	2.1	2.8	3.2	2.7	2.2
p-value		—	2.0E−1	4.0E−138	3.4E−200	2.0E−126	9.2E−35
Fold 5	**2.0**	**2.0**	2.1	2.5	3.4	2.3	2.6
p-value		—	8.2E−2	1.4E−73	1.4E−270	3.0E−48	1.5E−108

Table A6
Mean Absolute Percentage Error (%) of SINet and Related Methods on F30 Prediction (at 27th Day of Forecast)

	$SINet_f$	$SINet_r$	ARIMA	LSTM	CNN	LSTM+	TCN
Fold 1	**7.1**	7.9	7.7	8.4	8.2	7.8	7.4
p-value		1.5E−29	2.9E−2	5.0E−43	1.4E−49	2.1E−140	5.2E−187
Fold 2	**7.2**	7.9	7.6	8.7	8.0	7.5	7.6
p-value		1.0E−25	3.8E−2	8.1E−65	1.2E−62	2.3E−65	1.5E−265
Fold 3	**7.1**	7.9	7.5	8.5	8.2	7.6	7.7
p-value		2.0E−26	5.8E−3	3.0E−53	2.3E−105	8.3E−37	1.5E−151
Fold 4	**7.1**	7.9	7.5	8.5	8.3	7.6	7.3
p-value		1.2E−41	4.8E−3	7.3E−48	6.6E−70	3.8E−71	3.2E−114
Fold 5	**7.2**	7.8	7.5	8.5	8.3	7.5	7.5
p-value		3.8E−52	1.4E−2	6.2E−40	1.3E−64	2.0E−51	1.5E−65

Table A7
Mean Absolute Percentage Error (%) of SINet and Related Methods on F30 Prediction (at 45th Day of Forecast)

	$SINet_f$	$SINet_r$	ARIMA	LSTM	CNN	LSTM+	TCN
Fold 1	**8.7**	8.8	10.6	10.4	**8.7**	10.0	9.0
p-value		1.2E−1	6.8E−15	4.8E−67	—	1.4E−160	2.5E−219
Fold 2	**8.7**	9.0	10.6	10.6	9.0	10.2	9.2
p-value		1.4E−2	2.1E−17	1.5E−145	5.6E−41	1.4E−131	4.4E−28
Fold 3	**8.8**	8.9	10.5	10.5	**8.8**	10.0	9.0
p-value		1.8E−2	8.1E−16	1.9E−195	—	2.1E−172	1.4E−187
Fold 4	8.8	**8.7**	10.5	10.5	9.1	9.6	9.1
p-value		4.8E−1	3.1E−17	3.5E−76	5.1E−54	2.2E−113	2.5E−46
Fold 5	**8.7**	9.1	10.5	10.8	9.4	9.7	9.7
p-value		5.5E−9	1.3E−17	4.4E−89	2.0E−18	2.8E−164	3.9E−281

Table A8
Mean Absolute Percentage Error (%) of SINet and Related Methods on F30 Prediction (at 60th Day of Forecast)

	$SINet_f$	$SINet_r$	ARIMA	LSTM	CNN	LSTM+	TCN
Fold 1	**9.5**	9.6	10.7	10.3	10.3	9.6	9.6
p-value		7.4E−32	6.1E−10	3.3E−85	9.6E−37	9.0E−25	1.4E−11
Fold 2	**9.6**	10.4	10.7	10.2	10.1	9.7	**9.6**
p-value		1.6E−9	2.5E−8	7.9E−71	2.2E−35	1.1E−20	—
Fold 3	9.5	10.2	10.7	10.2	10.2	9.6	**9.4**
p-value		4.8E−22	8.9E−9	1.9E−298	9.3E−46	4.2E−18	8.8E−26
Fold 4	**9.5**	10.1	10.7	10.5	10.1	9.6	9.6
p-value		9.7E−25	6.6E−10	1.4E−36	1.9E−49	2.0E−21	4.0E−19
Fold 5	9.6	10.7	10.7	10.3	10.3	**9.5**	9.7
p-value		5.8E−45	1.5E−9	7.9E−117	1.1E−35	9.6E−21	1.2E−5

Conflict of Interest

The authors declare no conflicts of interest relevant to this study.

Data Availability Statement

The F10.7 solar index data are available from the NOAA/SWPC F10.7 cm radio emissions archive at https://www.swpc.noaa.gov/phenomena/f107-cm-radio-emissions. The F30 solar index data are available from the daily flux archive of the Nobeyama Radio Polarimeters at https://lasp.colorado.edu/lisird/data/cls_radio_flux_f30.

Acknowledgments
We are grateful to the anonymous referees for their valuable comments and constructive suggestions that have helped improve the manuscript significantly. We also thank members of the Institute for Space Weather Sciences for fruitful discussions. The SINet model was implemented in PyTorch. This work was supported in part by NSF Grants AGS-2149748, AGS-2228996, AGS-2300341, OAC-2320147, RISE-2425602, OAC-2504860, and NASA Grants 80NSSC24K0548, 80NSSC24K0843, and 80NSSC24M0174.

References

Abduallah, Y., Wang, J. T. L., Wang, H., & Xu, Y. (2023). Operational prediction of solar flares using a transformer-based framework. *Scientific Reports*, *13*(1), 13665. https://doi.org/10.1038/s41598-023-40884-1

Alobaid, K. A., Wang, J. T. L., Wang, H., Jing, J., Abduallah, Y., Wang, Z., et al. (2024). Prediction of geoeffective CMEs using SOHO images and deep learning. *Solar Physics*, *299*(11), 159. https://doi.org/10.1007/s11207-024-02385-w

Bernoux, G., Brunet, A., Buchlin, É., Janvier, M., & Sicard, A. (2022). Forecasting the geomagnetic activity several days in advance using neural networks driven by solar EUV imaging. *Journal of Geophysical Research (Space Physics)*, *127*(10), e2022JA030868. https://doi.org/10.1029/2022JA030868

Box, G. E., & Jenkins, G. M. (1970). *Time series analysis: Forecasting and control*. Holden Day.

Daniell, J. D., & Mehta, P. M. (2023). Probabilistic solar proxy forecasting with neural network ensembles. *Space Weather*, *21*(9), e2023SW003675. https://doi.org/10.1029/2023SW003675

Dudok de Wit, T., & Bruinsma, S. (2017). The 30 cm radio flux as a solar proxy for thermosphere density modelling. *Journal of Space Weather and Space Climate*, *7*, A9. https://doi.org/10.1051/swsc/2017008

Dudok de Wit, T., Kopp, G., Shapiro, A., Witzke, V., & Kretzschmar, M. (2018). Response of solar irradiance to sunspot-area variations. *The Astrophysical Journal*, *853*(2), 197. https://doi.org/10.3847/1538-4357/aa9f19

Fahim, M., & Sillitti, A. (2019). Anomaly detection, analysis and prediction techniques in IoT environment: A systematic literature review. *IEEE Access*, *7*, 81664–81681. https://doi.org/10.1109/ACCESS.2019.2921912

Girazian, Z., & Withers, P. (2015). An empirical model of the extreme ultraviolet solar spectrum as a function of $F_{10.7}$. *Journal of Geophysical Research (Space Physics)*, *120*(8), 6779–6794. https://doi.org/10.1002/2015JA021436

Hao, Y., Lu, J., Peng, G., Wang, M., Li, J., & Wei, G. (2024). $F_{10.7}$ daily forecast using LSTM combined with VMD method. *Space Weather*, *22*(1), e2023SW003552. https://doi.org/10.1029/2023SW003552

Hochreiter, S., & Schmidhuber, J. (1997). Long short-term memory. *Neural Computation*, *9*(8), 1735–1780. https://doi.org/10.1162/NECO.1997.9.8.1735

Jerse, G., & Marcucci, A. (2024). Deep learning LSTM-Based approaches for 10.7 cm solar radio flux forecasting up to 45-days. *Astronomy and Computing*, *46*, 100786. https://doi.org/10.1016/J.ASCOM.2024.100786

Jiang, H., Li, Q., Wang, J. T. L., Wang, H., & Criscuoli, S. (2025). Reconstruction of solar extreme-ultraviolet irradiance using Ca II K images and SOHO/SEM data with Bayesian deep learning and uncertainty quantification. *The Astrophysical Journal - Supplement Series*, *280*(2), 50. https://doi.org/10.3847/1538-4365/adfa0d

Kingma, D. P., & Ba, J. (2015). Adam: A method for stochastic optimization. In *Proceedings of the third international conference on learning representations*. Retrieved from http://arxiv.org/abs/1412.6980

Laštovička, J., & Burešová, D. (2023). Relationships between foF2 and various solar activity proxies. *Space Weather*, *21*(4), e2022SW003359. https://doi.org/10.1029/2022SW003359

LeCun, Y., Bottou, L., Bengio, Y., & Haffner, P. (1998). Gradient-based learning applied to document recognition. *Proceedings of the IEEE*, *86*(11), 2278–2324. https://doi.org/10.1109/5.726791

Lei, L., Zhong, Q., Wang, J., Shi, L., & Liu, S. (2019). The mid-term forecast method of F10.7 based on extreme ultraviolet images. *Advances in Astronomy*, *2019*, 5604092. https://doi.org/10.1155/2019/5604092

Myttenaere, A. D., Golden, B., Grand, B. L., & Rossi, F. (2016). Mean absolute percentage error for regression models. *Neurocomputing*, *192*, 38–48. https://doi.org/10.1016/J.NEUCOM.2015.12.114

Pedregosa, F., Varoquaux, G., Gramfort, A., Michel, V., Thirion, B., Grisel, O., et al. (2011). Scikit-learn: Machine learning in Python. J. *Mach. Learn. Res.*, *12*, 2825–2830. https://doi.org/10.5555/1953048.2078195

Petrova, E., Podladchikova, T., Veronig, A. M., Lemmens, S., Bastida Virgili, B., & Flohrer, T. (2021). Medium-term predictions of F10.7 and F30 cm solar radio flux with the adaptive Kalman filter. *The Astrophysical Journal - Supplement Series*, *254*(1), 9. https://doi.org/10.3847/1538-4365/abef6d

Preminger, D. G., & Walton, S. R. (2005). A new model of total solar irradiance based on sunspot areas. *Geophysical Research Letters*, *32*(14), L14109. https://doi.org/10.1029/2005GL022839

Tapping, K. F. (2013). The 10.7 cm solar radio flux ($F_{10.7}$). *Space Weather*, *11*(7), 394–406. https://doi.org/10.1002/swe.20064

Tasistro-Hart, A., Grayver, A., & Kuvshinov, A. (2021). Probabilistic geomagnetic storm forecasting via deep learning. *Journal of Geophysical Research (Space Physics)*, *126*(1), e28228. https://doi.org/10.1029/2020JA028228

Vaswani, A., Shazeer, N., Parmar, N., Uszkoreit, J., Jones, L., Gomez, A. N., et al. (2017). Attention is all you need. In *Proceedings of the annual conference on neural information processing systems*. Retrieved from https://proceedings.neurips.cc/paper/2017/hash/3f5ee243547dee91fbd053c1c4a845aa-Abstract.html

Wang, L., Zhang, H., Zhang, X., Peng, G., Li, Z., & Xu, X. (2024). Deep temporal convolutional networks for F10.7 radiation flux short-term forecasting. *Annales Geophysicae*, *42*(1), 91–101. https://doi.org/10.5194/angeo-42-91-2024

Warren, H. P., Emmert, J. T., & Crump, N. A. (2017). Linear forecasting of the F10.7 proxy for solar activity. *Space Weather*, *15*(8), 1039–1051. https://doi.org/10.1002/2017SW001637

Wilcoxon, F. (1945). Individual comparisons by ranking methods. *Biometric Bulletin*, *1*(6), 80–83. https://doi.org/10.2307/3001968

Wu, H., Hu, T., Liu, Y., Zhou, H., Wang, J., & Long, M. (2023). TimesNet: Temporal 2D-variation modeling for general time series analysis. In *Proceedings of the eleventh international conference on learning representations*. Retrieved from https://arxiv.org/abs/2210.02186

Xu, D., Sun, P., Feng, S., Liang, B., & Dai, W. (2025). Solar flare forecasting using hybrid neural networks. *The Astrophysical Journal - Supplement Series*, *276*(2), 68. https://doi.org/10.3847/1538-4365/ada281

Zhang, H., Jing, J., Wang, J. T. L., Wang, H., Abduallah, Y., Xu, Y., et al. (2025). Prediction of halo coronal mass ejections using SDO/HMI vector magnetic data products and a transformer model. *The Astrophysical Journal*, *981*(1), 37. https://doi.org/10.3847/1538-4357/adafa0

Zhang, K., Zuo, P., Zou, Z., Feng, X., Huang, Y., Wang, S., et al. (2024). Forecasting medium-term F10.7 using the deep-learning Informer model. *Solar Physics*, *299*(4), 47. https://doi.org/10.1007/s11207-024-02284-0

Zhu, H., Zhu, W., & He, M. (2022). Solar cycle 25 prediction using an optimized long short-term memory mode with F10.7. *Solar Physics*, *297*(12), 157. https://doi.org/10.1007/s11207-022-02091-5